

Article

A Novel Parameter Identification Algorithm for 3-DOF Ship Maneuvering Modelling Using Nonlinear Multi-Innovation

Baigang Zhao , Xianku Zhang *  and Cailei Liang

Navigation College, Dalian Maritime University, Dalian 116026, China; zbg87@dlmu.edu.cn (B.Z.); cailei_liang@dlmu.edu.cn (C.L.)

* Correspondence: zhangxk@dlmu.edu.cn

Abstract: In order to further explore more efficient identification algorithms that can solve the ship motion identification modeling problem, a novel identification algorithm for 3-DOF ship maneuvering modeling is proposed in this paper. Based on the recursive least-squares method, the proposed algorithm combines multi-innovation and nonlinear innovation techniques that focus on the innovation's processing. In addition, its convergence capability is theoretically demonstrated. The identification algorithm shows good accuracy and convergence that is verified by a simulation experiment on a container ship. Furthermore, another simulation experiment using the full mission ship handling simulator demonstrates its generalization capability.

Keywords: parameter identification; 3-DOF; ship maneuvering model; nonlinear multi-innovation



Citation: Zhao, B.; Zhang, X.; Liang, C. A Novel Parameter Identification Algorithm for 3-DOF Ship Maneuvering Modelling Using Nonlinear Multi-Innovation. *J. Mar. Sci. Eng.* **2022**, *10*, 581. <https://doi.org/10.3390/jmse10050581>

Academic Editors: Md Jahir Rizvi and Sergei Chernyi

Received: 31 March 2022

Accepted: 23 April 2022

Published: 25 April 2022

Publisher's Note: MDPI stays neutral with regard to jurisdictional claims in published maps and institutional affiliations.



Copyright: © 2022 by the authors. Licensee MDPI, Basel, Switzerland. This article is an open access article distributed under the terms and conditions of the Creative Commons Attribution (CC BY) license (<https://creativecommons.org/licenses/by/4.0/>).

1. Introduction

Ship mathematical models are the basis of ship maneuverability, ship motion control, and navigation simulation. In 2002, the International Maritime Organization (IMO) adopted the resolution of MSC.137(76) "Standards for Ship Maneuverability". The test of ship maneuverability is described as follows: "scale model tests and/or computer predictions using mathematical models can be performed to predict compliance at the design stage [1]". It is stipulated that mathematical models and computer simulations can be used to study ship maneuverability. Therefore, it is of great theoretical and practical significance to establish an accurate ship mathematical model. The process of establishing a mathematical model of ship motion is called ship motion modeling [2].

Ship motion is a complex process affected by multivariable coupling, multifactor interference, complex fluid dynamics, random uncertainty, etc. [3]. At present, the main modeling methods of ship motion include model tests, empirical formulas, mechanism modeling, and system identification. However, the economic and time costs of ship modeling tests are high, the modeling accuracy of the empirical formula method is low, manual debugging is cumbersome, and the application of mechanical modeling requires extensive computing resources and manual experience [4]. As an important branch of modern control theory, system identification has become an important method to establish the mathematical model of the controlled plant. The system identification method has the advantages of being simple, efficient, easy to operate, and can realize online modeling, especially in ship motion modeling, and thus has gradually become an important research method of ship motion modeling.

Among the ship identification modeling algorithms, the least-squares (LS) method, as a basic algorithm, has a wide range of applications [5,6]. However, LS has overfitting and matrix inverse problems, with the main limitations being the implementability and computation complexity of matrix inverse. The recursive least-squares (RLS) [7] algorithm avoids matrix inversion and can realize online identification. Its core idea is to use the current error (innovation) to modify the estimated value of the previous moment, then provide a

P-type learning rate [8] and dynamic forgetting factor λ [9] to adjust the weight of a single innovation and multi-innovation algorithm (MI) [10] to reuse multiple innovations [11], etc. and improve the identification accuracy and convergence speed. Thus, it can be seen that the processing of innovation may be further improved with this kind of algorithm. The Kalman filter (KF) is also widely used in the identification of ship models, and algorithms such as the extended Kalman filter (EKF) [12] and untracked Kalman filter (UKF) [13] have emerged. These algorithms have good identification effects for nonlinear systems, but there are also problems with parameter drift and dynamic cancellation. Support vector machine (SVM), as a new generation of machine learning theory, has also been used in ship model identification with typical ε -SVM, least squares support vector machine (LS-SVM), etc. [14]. These algorithms have complete theoretical derivation, strong generalization capabilities, global optimality, and other characteristics [15]. However, the training time of SVM can be very long when there is a large amount of data. In addition, the selection of kernel function and its parameters depends on experience, which is relatively random [16]. A Neural network (NN) is a kind of artificial intelligence algorithm that is similar to the human brain. Its remarkable characteristic of good nonlinear function approximation ability provides an effective way for the identification of nonlinear ship dynamics, moreover, it is easier for the algorithm to achieve online identification [17], but the neural network faces the problem of having a large number of ship calculations. In addition, in recent years, a class of improved multi-information (MI) [18] and nonlinear innovation [19,20] algorithms have emerged, which have improved the identification accuracy and convergence speed by processing the innovation (error information) based on some traditional identification algorithms. To sum up, in this paper, we focus on nonlinear multi-innovation technology based on the RLS algorithm and prove its identification effect and generalization capability using simulation experiments.

This paper is organized as follows: Section 2 introduces the MMG model of the ship, which is used as an identification object and to produce identification data; Section 3 describes the novel identification algorithm, namely, the nonlinear multi-innovation recursive least-squares (NMI-RLS) algorithm; Section 4 demonstrates the convergence of this algorithm; Section 5 is the simulation and analysis, where the identification effect of the algorithm is verified and its generalization capability is demonstrated; and Section 6 is the conclusion.

2. Ship Maneuvering Model

The MMG model is a set of systematic, comprehensive, and commonly used ship motion models proposed by the Japan Towing Tank Commission (JTTC) [21]. From a physical perspective, the MMG model decomposes the hydrodynamic force and torque acting on the hull into those acting on the hull, propeller, and rudder, and considers the interaction among them. A four-degree-of-freedom (4-DOF) mathematical model of ship motion is established to describe the motion of a ship without considering the heave and pitch. The MMG model is usually used in autopilot design, simulation experiments, ship anti-roll, collision avoidance, and dynamic positioning (DP) controller design [22]. Accuracy is sufficient when studying the above problems. Figure 1 shows the coordinate system used in this article. Consider the coordinate system O-XYZ fixed on the earth, where the O-X-Y plane coincides with the static water surface and the O-Z axis is straight down. In addition, consider the horizontal body-fixed coordinate system O-XYZ. The x -axis is the bow direction, the y -axis is transverse, and the z -axis is vertical downward. The x - y plane also coincides with the static water surface. Therefore, the origin O is located in the middle of the ship on the still water surface [23]. In fact, the accuracy of the 3-DOF model is sufficient in collision avoidance, course control, path-following, and track keeping. The main purpose of this paper was to verify the effectiveness of the proposed identification

algorithm. Therefore, the 4-DOF model was simplified to 3-DOF, which was adopted as the research object. The 3-DOF mathematical descriptions were as follows:

$$\begin{cases} (m + m_x)\dot{u} - (m + m_y)vr = X_H + X_p + X_R \\ (m + m_y)\dot{v} + (m + m_x)ur = Y_H + Y_p + Y_R \\ (I_{zz} + J_{zz})\dot{r} = N_H + N_p + N_R \end{cases} \quad (1)$$

$$\begin{cases} \dot{x} = u \cos(\psi) - v \sin(\psi) \\ \dot{y} = u \sin(\psi) + v \cos(\psi) \\ \dot{\psi} = r \cos(\varphi) \end{cases} \quad (2)$$

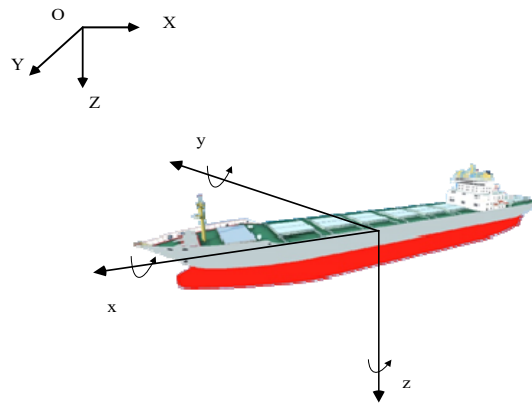


Figure 1. Coordinate systems for ships motion.

In Equations (1) and (2), u, v denote surge velocity and lateral velocity, r denotes yaw rate, m denotes ship mass, m_x denotes added masses of the x -axis direction, m_y denotes added masses of the y -axis direction, I_{zz} is for the inertia of the ship about the x -axis, while J_{zz} is for the added moment of inertia about the x -axis. $X_{H,P,R}, Y_{H,P,R}$ denote forces and $N_{H,P,R}$ denotes the moment acting on the ship. (x, y) is the position of the ship, and ψ denotes the heading.

Then, based on previous research, the hydrodynamic forces and moments can be given as the identification model.

(1) Hydrodynamics force and moments

$$\begin{cases} X_H = X_{uu}u^2 + X_{uuu}u^3 + X_{vv}v^2 + X_{rr}r^2 + X_{vr}vr + X_{uv^2}uv^2 + X_{uvr}uvr + X_{ur^2}ur^2 \\ Y_H = Y_{uv}uv + Y_{ur}ur + Y_{uur}u^2r + Y_{uuv}u^2v + Y_{vvv}v^3 + Y_{rrr}r^3 + Y_{vrr}vr^2 + \\ Y_{vvr}v^2r + Y_{v|v|}v|v| + Y_{v|r|}v|r| + Y_{r|v|}r|v| + Y_{r|r|}r|r| \\ N_H = N_{uv}uv + N_{ur}ur + N_{uur}u^2r + N_{uuv}u^2v + N_{vvv}v^3 + N_{rrr}r^3 + \\ N_{vvr}v^2r + N_{vrr}vr^2 + N_{r|r|}r|r| + N_{|v|v|}v|v| + N_{|r|v|}r|v| + N_{|v|r|}v|r| \end{cases} \quad (3)$$

Therefore, in this study, the following hydrodynamic derivatives will be identified:

$$\begin{cases} X_H : X_{uu}, X_{uuu}, X_{vv}, X_{rr}, X_{vr}, X_{uvv}, X_{uvr}, X_{urr}; \\ Y_H : Y_{uv}, Y_{ur}, Y_{uur}, Y_{uuv}, Y_{vvv}, Y_{rrr}, Y_{vrr}, Y_{vvr}, Y_{v|v|}, Y_{v|r|}, Y_{r|v|}, Y_{r|r|}; \\ N_H : N_{uv}, N_{ur}, N_{uur}, N_{uuv}, N_{vvv}, N_{rrr}, N_{vvr}, N_{vrr}, N_{r|r|}, N_{|v|v|}, N_{|r|v|}, N_{|v|r|}. \end{cases}$$

(2) Propeller forces and moments

$$\begin{cases} X_p = (1 - t_p)T \\ Y_p = 0 \\ K_p = 0 \\ N_p = 0 \end{cases} \quad (4)$$

$$T = \rho n^2 D_p^4 k_T (J_p) \quad (5)$$

In Equations (4) and (5), t_p, ρ, n, D_p denote thrust deduction fraction, water density, propeller revolution, and propeller diameter, respectively.

$$k_T(J_P) = a_0 + a_1 J_P + a_2 J_P^2 \tag{6}$$

In Equation (6), a_0, a_1, a_2 are constant, $J_p = (1 - w_p)u/nD_p$, w_p denotes wake fraction at the propeller position in maneuvering motions.

(3) Rudder force and moment (X_R, Y_R, K_R, N_R)

$$\begin{cases} X_R = -(1 - t_R)F_N \sin(\delta) \\ Y_R = -(1 - a_H)F_N \cos(\delta) \\ N_R = -(x_R + a_H x_H)F_N \cos(\delta) \end{cases} \tag{7}$$

$$F_N = \frac{1}{2}\rho V_R^2 A_R f_\alpha \sin(\alpha_R) \tag{8}$$

$$f_\alpha = 6.13\lambda_R / (2.25 + \lambda_R) \tag{9}$$

In Equations (7)–(9), $V_R, A_R, \lambda_R, \alpha_R, C_b$ denote current velocity, rudder profile area, aspect ratio, the effective angle of current, and block coefficient, respectively.

$$\begin{cases} t_R = 0.2168 + 0.00539C_b - 0.1755C_b^2 \\ a_H = 0.6784 - 1.3374C_b + 1.8891C_b^2 \\ x_R \approx -0.5L \\ x_H = -(0.4 + 0.1C_b)L \\ z_R \approx z_H = 0.4d \end{cases} \tag{10}$$

For the convenience of identification, the Equations (1)–(10) were rewritten as follows:

$$\begin{aligned} Z_u(V, t) &:= (m + m_x)\dot{u} - (m + m_y)vr, \\ Z_v(V, t) &:= (m + m_y)\dot{v} + (m + m_x)ur, \\ Z_r(V, t) &:= (I_z + J_z)\dot{r}, V = [u, v, p, r]^T \end{aligned} \tag{11}$$

$$\begin{aligned} \varphi_u(V, t) &= [u^2, u^3, \dots, T(J_p), -F_N \sin \delta]^T \in R^{8 \times 1}, \\ \varphi_v(V, t) &= [uv, ur, \dots, |r|r, -F_N \cos \delta]^T \in R^{12 \times 1}, \\ \varphi_r(V, t) &= \varphi_v(V, t) \end{aligned} \tag{12}$$

$$\begin{aligned} \vartheta_u &= [X_{uu}, X_{uuu}, \dots, C_P, C_{Ru}]^T, \\ \vartheta_v &= [Y_{uv}, Y_{ur}, \dots, Y_{|r|r}, C_{Rv}]^T, \\ \vartheta_r &= [N_{uv}, N_{ur}, \dots, N_{|r|r}, C_{Rr}]^T, \\ C_P &= 1 - t_p, C_{Ru} = 1 - t_R, C_{Rv} = 1 + a_H, \\ C_{Rr} &= x_R + a_H x_H \end{aligned} \tag{13}$$

$$Z_i(V, t) = \varphi_i^T(V, t)\vartheta_i + \omega_i(t), i = u, v, r \tag{14}$$

In Equation (14), $Z_i(V, t), \varphi_i(V, t)$ are the output scalar and the information vectors that consist of the measured ship maneuvering motion variables at a time, $\omega_i(t)$ is the noise term.

3. Parameter Identification Algorithm Using Nonlinear Multi-Innovation

The least-square (LS) method is a mature application in system identification, which is simple and reliable and has good identification abilities. However, in general, least squares face overfitting and matrix-inversion problems. Matrix inversion, in particular, is a problem as not all matrices are invertible and the matrix inversion calculation is large. In addition, the LS method is unable to realize online identification. Therefore, the recursive least-squares (RLS) algorithm was developed, which is an improved algorithm of LS, and it

became one of the most common identification algorithms. The general application of its identification algorithm [11] is as follows:

$$\begin{aligned} \hat{\theta}(t) &= \hat{\theta}(t-1) + P(t)\varphi(t)e(t) \\ e(t) &= Z(t) - \varphi^T(t)\hat{\theta}(t-1) \\ P^{-1}(t) &= P^{-1}(t-1) + \varphi(t)\varphi^T(t) \end{aligned} \tag{15}$$

In Equation (15); $\hat{\theta}(t)$ is the estimated value of θ at time t ; $P(t)$ is covariance matrix; $e(t)$ is the innovation scalar for each iteration. Initial values of identification parameters and covariance matrix were set as:

$$\begin{aligned} \hat{\theta}(0) &= \mathbf{1}_n / p_0 \\ P(0) &= p_0 * I \end{aligned} \tag{16}$$

here, $p_0 > 1$ and constant, generally is 10^6 ; $\mathbf{1}_n$ is a column vector of length n with all elements 1; I is a unit diagonal matrix.

From the perspective of parameter recursive identification, $P(t)\varphi(t)$ is a gain matrix in Equation (15), which revises the innovation $e(t)$, $e(t)$ is the error between the actual output $Z(t)$ and the estimated value $\varphi^T(t)\hat{\theta}(t-1)$ produced by the identification parameters of the previous moment. Therefore, the whole recursion process only uses the input and output data at the current time t , which can be regarded as the single innovation least-squares method. In order to increase the efficiency of old innovation and improve the accuracy and convergence of RLS, the innovation scalar $e(t)$ in Equation (15) was extended to a multi-innovation vector $E(l, t)$ with length l . As shown in Equation (17):

$$E(l, t) = \begin{bmatrix} e(t) \\ e(t-1) \\ \vdots \\ e(t-l+1) \end{bmatrix} = \begin{bmatrix} Z(t) - \varphi(t)^T\theta \\ Z(t-1) - \varphi(t-1)^T\theta \\ \vdots \\ Z(t-l+1) - \varphi(t-l+1)^T\theta \end{bmatrix} \tag{17}$$

Similarly, the information vector and output vector were also extended to:

$$\begin{aligned} Z(l, t) &= [Z(t), Z(t-1), \dots, Z(t-l+1)]^T \in R^{l \times 1}, \\ \Phi(l, t) &= [\varphi(t), \varphi(t-1), \dots, \varphi(t-l+1)] \in R^{n \times l} \end{aligned} \tag{18}$$

and then substituting the extended matrix into Equation (15), we can obtain:

$$E(l, t) = Z(l, t) - \Phi^T(l, t)\hat{\theta}(t-1) \tag{19}$$

Then, Equation (19) can be improved by multi-innovation, and we can obtain the multi-innovation recursive least-squares (MI-RLS) as shown:

$$\begin{aligned} \hat{\theta}(t) &= \hat{\theta}(t-1) + L(t)[Z(l, t) - \Phi^T(l, t)\hat{\theta}(t-1)], \\ L(t) &= P(t-1)\Phi(l, t)[I_l + \Phi^T(l, t)P(t-1)\Phi(l, t)]^{-1}, \\ P(t) &= P(t-1) - L(t)\Phi^T(l, t)P(t-1) \end{aligned} \tag{20}$$

According to the authors' previous research [19,20], the nonlinear innovation is a kind of improved algorithm based on innovation. In this paper, the MI-RLS was improved by the idea of nonlinear, as shown below:

$$Z(l, t) = N * E(l, t) = N * [Y(l, t) - \Phi^T(l, t)\hat{\theta}(t-1)] \tag{21}$$

Here, N denotes the nonlinear function, which is applied to decorate the multi-innovation, in this paper, this nonlinear function is $f(e) = \sin(\omega e)$. To sum up, Equation (20) was finally transformed into (NMI-RLS):

$$\begin{aligned} \hat{\theta}(t) &= \hat{\theta}(t-1) + P(t)\Phi(l,t)Z(l,t) \\ Z(l,t) &= \sin(\omega(Y(l,t) - \Phi^T(l,t)\hat{\theta}(t-1))) \\ P^{-1}(t+1) &= P^{-1}(t) + \Phi(l,t+1)\Phi^T(l,t+1) \end{aligned} \tag{22}$$

as for covariance matrix P , which can also be expressed in another form:

$$P(t+1) = P(t) + \frac{[P(t)\Phi(l,t+1)][P(t)\Phi(l,t+1)]^T}{1 + \Phi^T(l,t+1)P(t)\Phi(l,t+1)} \tag{23}$$

4. Convergence Analysis of the NMI-RLS

Let $\tilde{\theta}_k(t) = \hat{\theta}_k(t) - \theta$, here the superscript “ \sim ” represents the error between the estimated value and the actual value, and the superscript “ $\hat{}$ ” represents the estimated value. k is the number of iterations [8]. Then,

$$\tilde{\theta}_k(t) - \tilde{\theta}_{k-1}(t) = \hat{\theta}_k(t) - \hat{\theta}_{k-1}(t) = \frac{P_{k-1}(t)\Phi_k(l,t)}{1 + \Phi_k^T(l,t)P_{k-1}(t)\Phi_k(l,t)}Z_k(l,t) + \Phi_k(l,t)\hat{Z}_k(l,t) \tag{24}$$

and let

$$\chi_k(t) = \frac{1}{1 + \Phi_k^T(l,t)P_{k-1}(t)\Phi_k(l,t)} \tag{25}$$

according to Equations (18)–(23), then

$$P_k(t)\Phi_k(l,t) = \chi(t)P_{k-1}(t)\Phi_k(l,t) \tag{26}$$

$$Z_k(l,t) = Y_k(l,t) - \Phi_k^T(l,t)\hat{\theta}_{k-1}(t) = -\Phi_k^T(l,t)\tilde{\theta}_{k-1}(t) \tag{27}$$

$$\hat{Z}_k(l,t) = -\chi_k(t)\Phi_k^T(l,t)\tilde{\theta}_{k-1}(t) \tag{28}$$

Substituting Equations (27) and (28) into Equation (24), we can obtain:

$$\tilde{\theta}_k(t) = P_k(t)P_{k-1}^{-1}(t)\tilde{\theta}_{k-1}(t) - \chi_k(t)\Phi_k(t)\Phi_k^T(l,t)\tilde{\theta}_{k-1}(t) \tag{29}$$

Define the Lyapunov function:

$$V_k(t) = \tilde{\theta}_k^T(t)P_k^{-1}(t)\tilde{\theta}_k(t) \tag{30}$$

then:

$$\begin{aligned} V_k(t) - V_{k-1}(t) &= \\ \tilde{\theta}_k^T(t)P_k^{-1}(t)\tilde{\theta}_k(t) - \tilde{\theta}_{k-1}^T(t)P_{k-1}^{-1}(t)\tilde{\theta}_{k-1}(t) &= \\ A + B \end{aligned} \tag{31}$$

in Equation (31):

$$A = -\chi_k(t)\tilde{\theta}_{k-1}^T(t)\Phi_k(l,t)\Phi_k^T(l,t)\tilde{\theta}_{k-1}(t) \tag{32}$$

$$B = -\chi_k^2(t)\tilde{\theta}_{k-1}^T(t)\Phi_k(l,t)\Phi_k^T(l,t)\{2P_K^{-1} - 1(t) + [2I - P_k^{-1}]\Phi_k(l,t)\Phi_k^T(l,t)\}\tilde{\theta}_{k-1}(t) \tag{33}$$

According to Equation (32), we can know $A \leq 0$. As long as $B \leq 0$, the convergence of the algorithm can be proven according to Lyapunov’s law. In Equation (24), we can see

$$0 < \lambda(P_k(t)) < \lambda(P_{k-1}(t)) < \dots < \lambda(P_0(t)) < \lambda(P_0) = P_0 \tag{34}$$

is the biggest eigenvalue of $P_k(t)$, then

$$B = -\chi_k^2(t)\tilde{\theta}_{k-1}^T(t)\Phi_k(l,t)\Phi_k^T(l,t)\{2P_{k-1}^{-1} + [2 - P_0^{-1}]\Phi_k(l,t)\Phi_k^T(l,t)\}\tilde{\theta}_{k-1}(t) \tag{35}$$

because P_0 is a big positive constant, so $B < 0$, and

$$V_k(t) - V_{k-1}(t) = A + B < 0$$

Above all, the convergence capability of NMI-RLS was demonstrated.

5. Simulations and Analysis

In this paper, a set of simulation experiments were designed to verify the effectiveness and generalization capability of the proposed algorithm. First, a group of ship maneuverability tests were performed with predefined MMG models of a container ship containing disturbance (wind and wave) to generate identification data, and then the identification results were obtained by the proposed identification algorithm and identification data. The identification results were used to carry out similar maneuverability tests to verify the validity of the algorithm. Second, similar simulations were conducted on an ‘‘Own-ship 1’’ (OS 1) in the full mission ship handling simulator to further verify the generalization capability of the proposed algorithm.

5.1. Disturbance

In order to increase the credibility of simulation experiments, disturbances (wind and wave) were added to simulate the actual sea condition. The forces and moments produced by wind, which (X_A, Y_A, N_A) can be expressed as [24]:

$$\begin{aligned} X_A &= (1/2)\rho_a A_X V_A^2 C_{XA}(\theta_A) \\ Y_A &= (1/2)\rho_a A_Y V_A^2 C_{YA}(\theta_A) f_A(\phi) \\ N_A &= (1/2)\rho_a A_Y V_A^2 L C_{NA}(\theta_A) f_A(\phi) \end{aligned} \tag{36}$$

here

$$\begin{aligned} \theta_A &= \tan^{-1}(v_A/u_A) \\ V_A^2 &= u_A^2 + v_A^2 \\ u_A &= u + U_W \cos(\theta_W - \psi) \\ v_A &= v + U_W \sin(\theta_W - \psi) \end{aligned} \tag{37}$$

Here, ρ_a, A_X, A_Y denote the air density, front, and side profile areas of the ship above water, respectively. V_A, U_W denote the relative and absolute wind velocity, θ_A, θ_W are the relative and absolute wind direction. C_{XA}, C_{YA}, C_{NA} are aerodynamic force coefficients expressed as a function of θ_A . $f_A(\phi)$ denotes the correction coefficient expressed as $f_A = -0.355\phi + 1$ [23]. The forces and moments produced by waves, which (X_W, Y_W, N_W, K_W) are expressed as

$$\begin{aligned} X_W &= \rho g H_{1/3}^2 L \overline{C_{XW}}(U, T_P, \chi_0) \\ Y_W &= \rho g H_{1/3}^2 L \overline{C_{YW}}(T_P, \chi_0) \\ N_W &= \rho g H_{1/3}^2 L \overline{C_{NW}}(T_P, \chi_0) \end{aligned} \tag{38}$$

here $H_{1/3}, g$ denotes the wave height and gravitational acceleration. $\overline{C_{XW}}, \overline{C_{YW}}$ and $\overline{C_{NW}}$ denote steady force coefficients in waves. which can be expressed as:

$$\begin{aligned} \overline{C_{XW}}(U, T_P, \chi_0) &= 2 \int_{-\pi}^{\pi} G(\theta) d\theta \int_0^{\infty} \overline{C_{XW}}(U, T_P, \chi_0) \frac{S_{\zeta\zeta}(\omega)}{H_{1/3}^2} d\omega \\ \overline{C_{YW}}(T_P, \chi_0) &= 2 \int_{-\pi}^{\pi} G(\theta) d\theta \int_0^{\infty} \overline{C_{YW}}(\omega, \chi_0) \frac{S_{\zeta\zeta}(\omega)}{H_{1/3}^2} d\omega \\ \overline{C_{NW}}(T_P, \chi_0) &= 2 \int_{-\pi}^{\pi} G(\theta) d\theta \int_0^{\infty} \overline{C_{NW}}(\omega, \chi_0) \frac{S_{\zeta\zeta}(\omega)}{H_{1/3}^2} d\omega \end{aligned} \tag{39}$$

$S_{\zeta\zeta}(\omega)$ is the wave spectrum, and $G(\theta)$ is the wave direction distribution function.

According to Equations (36)–(39), the simulation experiments of this paper introduce the wind and wave under the fifth sea state as shown in Figure 2.

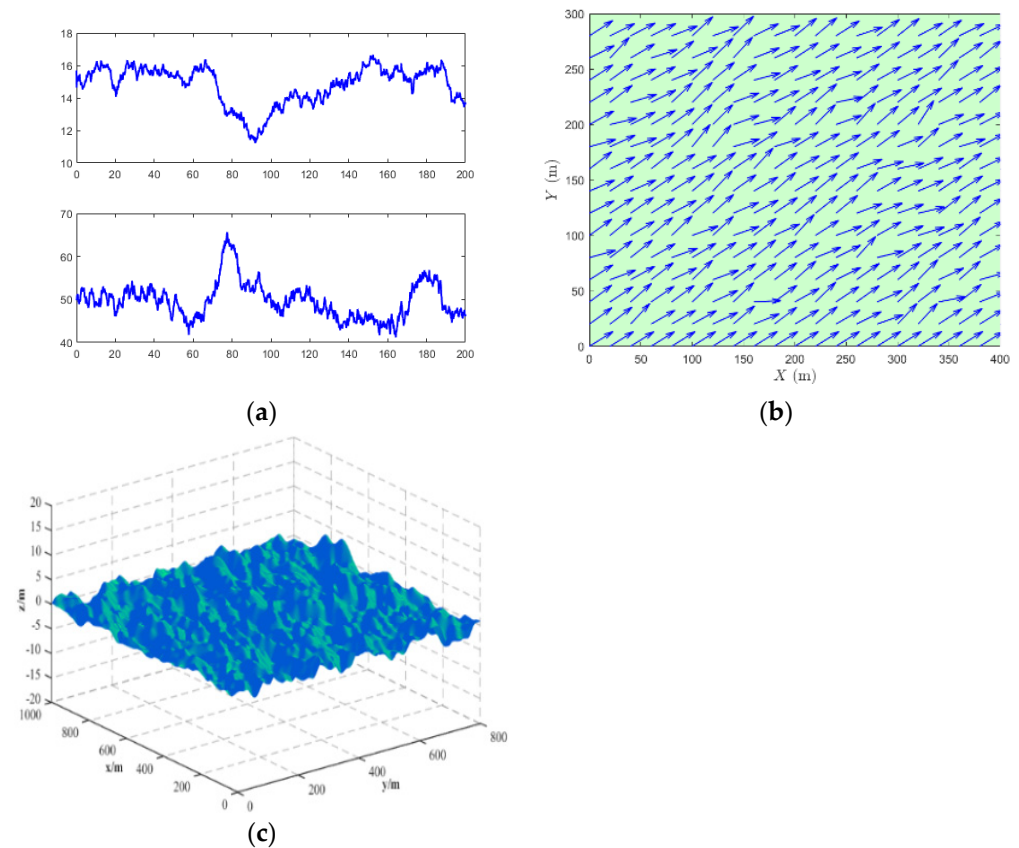


Figure 2. Environment disturbance in fifth sea state. (a,b) 2D planar graph of wind field. (c) Corresponding wind-generated wave.

5.2. The Effectiveness of the Proposed Algorithm (NMI-RLS)

In this section, we identify a known container ship to illustrate the effectiveness of proposed algorithm. To be specific, in the reference [18], a container ship was used in the simulation with the known model structure and parameters as shown in Table 1. In addition, a kind of multi-innovation least squares (MILS) was proposed. In this paper, we used the container ship and the MILS as comparative simulation experiments.

Table 1. The particulars of container ship.

Particulars of Container Ship		
Length between perpendiculars	L (m)	175.0
Breadth	B (m)	25.4
Designed draught	D (m)	8.5
Volume of displacement	∇ (m ³)	21,222.0
Block coefficient	C_b	0.559
Height from keel to transverse metacenter	KM (m)	10.39
Rudder area	A_R (m ²)	22.04
Aspect ratio	Δ	-0.51
Propeller diameter	D (m)	6.53

First, the container ship was employed to simulate the zig-zag test to produce motion data (identification data) as shown in Figure 3. Subsequently, we used the MILS method (proposed in reference [18]) and the nonlinear MI-RLS method (proposed in this paper) to evaluate the parameters of the container ship.

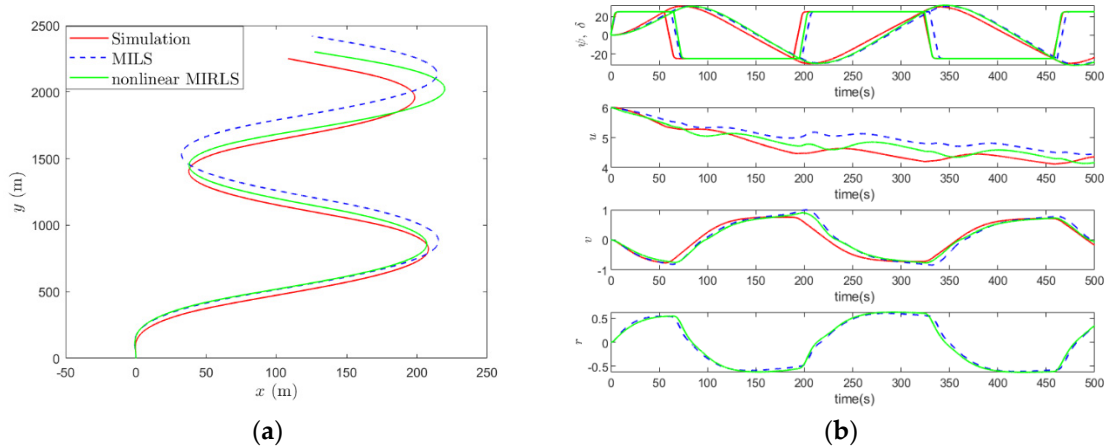


Figure 3. Identification results. (a) Zig-zag simulation (b) Motion variables.

As shown in Figure 3a, the zig-zag simulation experiments included the known model (red line), the MILS-based (dashed line), and the nonlinear MIRLS-based (green line) identified models. In the whole stage of simulations, the trajectory error of the MILS-based identification model response was always bigger than that of the nonlinear MIRLS-based identification model response, especially in the final stage, the trajectory error is significantly different.

Furthermore, the motion variables of the container ship under three different models (known, MILS, and nonlinear MI-RLS) are shown in Figure 3b, which included the rudder angle δ , the heading ψ , the longitudinal speed u , the lateral speed v , and the yaw rate r . Based on that, during the whole process, the green line is mostly between the red line and the dashed line. This demonstrates that the performance of the nonlinear MI-RLS method is better than the MILS method. In order to increase the reliability of simulation experiments and facilitate repetitive experiments, the final identified parameters (nonlinear MI-RLS) are given in Table 2.

Table 2. Identified hydrodynamic derivatives.

Parameter Identification for the Hydrodynamic Force		
$X_{uu} = -1.7269$	$Y_{uv} = 1.2316$	$N_{uv} = 0.0149$
$X_{uuu} = 1.7265$	$Y_{ur} = 2.0764$	$N_{ur} = -0.1533$
$X_{vv} = 4.0798$	$Y_{uur} = -2.0740$	$N_{uur} = 0.1525$
$X_{rr} = -1.4597$	$Y_{uuv} = -1.2372$	$N_{uuv} = -0.0142$
$X_{vr} = -1.5504$	$Y_{vvv} = 2.3357$	$N_{vvv} = -0.0126$
$X_{uvv} = -3.2796$	$Y_{rrr} = 0.0369$	$N_{rrr} = -0.0183$
$X_{uvr} = 1.5436$	$Y_{vrr} = 0.1787$	$N_{vrr} = -0.0695$
$X_{urr} = 1.4738$	$Y_{vvr} = 0.2364$	$N_{vvr} = -0.0054$
	$Y_{ v v} = -0.4871$	$N_{ v v} = -0.0089$
	$Y_{ r v} = -0.0634$	$N_{ r v} = 0.0017$
	$Y_{ v r} = -0.2374$	$N_{ v r} = -0.0121$
	$Y_{ r r} = -0.0139$	$N_{ r r} = 0.0056$

5.3. The Generalization Capability of the Proposed Algorithm

Full mission ship handling simulators have been developed for more than 20 years and have high-precision mathematical models with 6-DOF. The simulators are in full compliance with the STCW 2010, as shown in Figure 4. In particular, the full mission handling simulator has been approved by DNV (class A) and CCS. In this section, we chose a ship “own-ship 1” (OS 1) in the simulator. Then, a turning test and zig-zag test were conducted in the simulator and the trial data (identification data) were downloaded. It is noted that the ship model in the simulator is unknown. The ship model parameters are

identified using the trial data by the proposed nonlinear MI-RLS algorithm as shown in Table 3.



Figure 4. Full Mission Ship Handling Simulator.

Table 3. Identified hydrodynamic derivatives.

Parameter Identification for the Hydrodynamic Force		
$X_{uu} = -0.1374$	$Y_{uv} = -59.1666$	$N_{uv} = 22.5966$
$X_{uuu} = 0.1375$	$Y_{ur} = 26.7604$	$N_{ur} = -5.6630$
$X_{vv} = 0.2321$	$Y_{uur} = -26.7489$	$N_{uur} = 5.6549$
$X_{rr} = 0.0077$	$Y_{uuv} = 59.1594$	$N_{uuv} = -22.5931$
$X_{vr} = 0.3094$	$Y_{vvv} = 29.5338$	$N_{vvv} = -10.4279$
$X_{uvv} = -0.1937$	$Y_{rrr} = 0.0383$	$N_{rrr} = -0.3289$
$X_{uvr} = -0.3339$	$Y_{vrr} = -0.0830$	$N_{vrr} = -0.2950$
$X_{urr} = -0.0061$	$Y_{vvr} = -13.4274$	$N_{vvr} = 3.1337$
	$Y_{ v v} = -0.0610$	$N_{ v v} = -0.1388$
	$Y_{ r v} = 0.0323$	$N_{ r v} = 0.0048$
	$Y_{ v r} = -0.0130$	$N_{ v r} = -0.0260$
	$Y_{ r r} = -0.0139$	$N_{ r r} = 0.0878$

As shown in Figure 5, the trial experiment and identified model simulation are compared. It is clear that the turning circle generated by the identified model was smaller than that of the trial experiments. Because the disturbance in the simulation experiment and the simulator experiment was random, discrepancies have appeared between the trial results and the identified model, and with the increase of experiment time, these discrepancies will accumulate and become larger. However, in the initial stage, the error is minute. Figure 5b gives the longitudinal speed u , the lateral speed v and the yaw rate r and we can see that they are similar to each other. From the turning test simulation, the effectiveness of the proposed identification algorithm is satisfactory.

In order to make the generalization capability of the identification algorithm convincing, a zig-zag test was carried out to further verify the effectiveness of the proposed algorithm. As shown in Figure 6a, we see that the trial experiments and the identified model simulation had similarities, on the other hand, as shown in Figure 6b, the motion variables of the ship under the two different conditions also had good fitting properties. In general, a good generalization capability of the proposed algorithm was shown through the above two groups of comparative experiments.

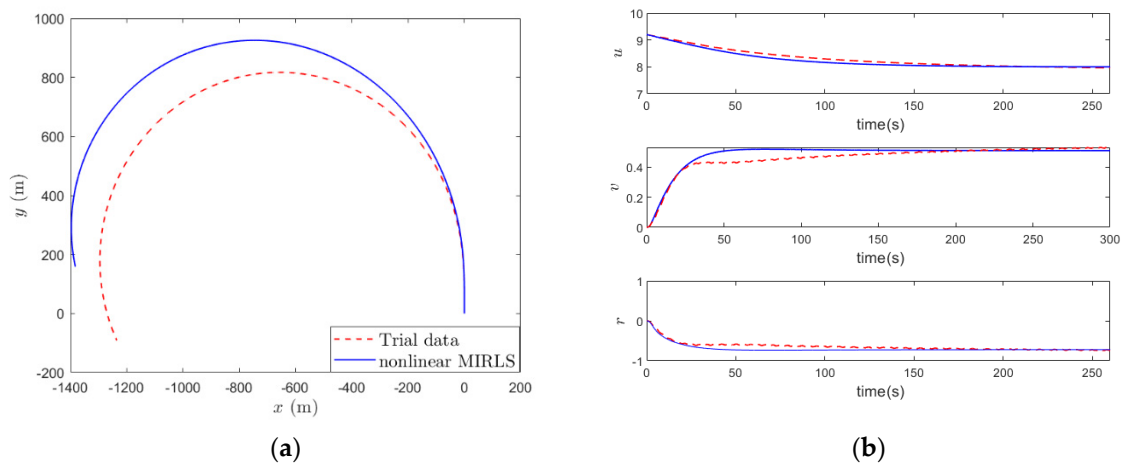


Figure 5. The comparison between the trial experiment and the identified model responses in the turning test. (a) Turning test simulation (b) Motion variables.

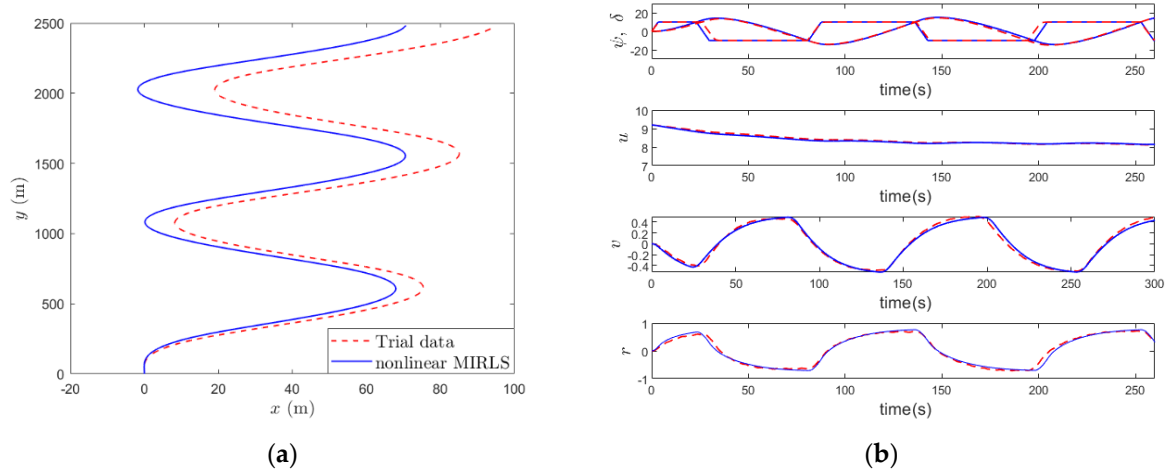


Figure 6. The comparison between the trial result and the identified model responses in the zig-zag test. (a) Zig-zag simulation (b) Motion variables.

6. Conclusions

In this paper, a nonlinear MI-RLS identification algorithm for the ship is proposed. Based on a traditional MILS identification algorithm, we employed a nonlinear function to decorate it. The convergence of the algorithm was theoretically demonstrated. Furthermore, we conducted an identification simulation using a container ship to verify the effectiveness, and another experiment in the full mission ship handling simulator to show generalization capability. The results obtained were satisfying in both tests. However, there were also some flaws in the proposed algorithm—we only identified a 3-DOF ship motion model, which could not be employed in roll control problems. Future studies will focus on this matter.

Author Contributions: Methodology, B.Z.; software, C.L.; writing—original draft preparation, B.Z.; writing—review and editing, X.Z.; supervision, X.Z. All authors have read and agreed to the published version of the manuscript.

Funding: This research was funded by the National Natural Science Foundation of China (grant number 51679024, 51909018) and the University 111 Project of China (grant number B08046).

Institutional Review Board Statement: Not applicable.

Informed Consent Statement: Not applicable.

Data Availability Statement: The data used to support the findings of this study are available from the corresponding author upon request.

Conflicts of Interest: The authors declare no conflict of interest.

References

- IMO. Standards for ship manoeuvrability. In *MSC 76th Session*; International Maritime Organization (IMO): London, UK, 2002; Volume MSC. 137, p. 6.
- Zhang, X.; Wang, X.; Meng, Y.; Yin, Y. Research progress and future development trend of ship motion modeling and simulation. *J. Dalian Marit. Univ.* **2021**, *47*, 1–8.
- Jia, X.; Yang, Y. *Ship Motion Mathematical Models*; Dalian Maritime University Press: Dalian, China, 1999.
- Mei, B. *Grey Box Identification Modeling for Ship Manoeuvring Motion Based on Free Running Test*; Doctor, Dalian Maritime University: Dalian, China, 2020.
- Schimmack, M.; Feistauer, E.E.; Amancio, S.T.; Mercorelli, P. Hysteresis analysis and control of a metal-polymer hybrid soft actuator. *Energies* **2017**, *10*, 508. [[CrossRef](#)]
- Schimmack, M.; Mercorelli, P.; Maiwald, M. Combining kalman filter and rls-algorithm to improve a textile based sensor system in the presence of linear time-varying parameters. In *Proceedings of the 2015 17th International Conference on E-Health Networking, Application & Services (Healthcom)*, Boston, MA, USA, 14–17 October 2015; pp. 507–510.
- Åström, K.J.; Källström, C. Identification on ship steering dynamics. *Automatica* **1976**, *12*, 4. [[CrossRef](#)]
- Qin, Y.; Ma, Y.; Zhang, L.; Li, T. Parameter identification of ship's maneuvering motion based on improved least squares method. *J. Jilin Univ. Eng. Technol. Ed.* **2016**, *46*, 897–903.
- Sun, G.; Xie, J.; Wang, J. Ship course identification model based on recursive least squares algorithm with dynamic forgetting factor. *J. Comput. Appl.* **2018**, *38*, 900–904.
- Xie, S.; Chu, X.; Liu, C.; Wu, Q. Parameter identification of ship maneuvering response model based on multi-innovation least squares algorithm. *China Navig.* **2017**, *40*, 73–78.
- Xie, S.; Chu, X.M.; Liu, C.G.; Liu, J.L.; Mou, J.M. Parameter identification of ship motion model based on multi-innovation methods. *J. Mar. Sci. Tech.-Jpn.* **2020**, *25*, 162–184. [[CrossRef](#)]
- Cao, W. *Ship Heading Model Parameter Identification Based on EKF and I2 Closed-Loop Forming Filter Control*; Dalian Maritime University: Dalian, China, 2020.
- Deng, F.; Yang, H.L.; Wang, L.J.; Yang, W.M. Ukf based nonlinear offset-free model predictive control for ship dynamic positioning under stochastic disturbances. *Int. J. Control Autom. Syst.* **2019**, *17*, 3079–3090. [[CrossRef](#)]
- Jiang, Y.; Wang, X.G.; Zou, Z.J.; Yang, Z.L. Identification of coupled response models for ship steering and roll motion using support vector machines. *Appl. Ocean Res.* **2021**, *110*, 3079–3090. [[CrossRef](#)]
- Wang, X. *On the Modeling of Ship Manoeuvring Motion in 4 Degrees of Freedom Based on Support Vector Machines*; Shanghai JiaoTong University: Shanghai, China, 2014.
- Dong, Z.P.; Yang, X.; Zheng, M.; Song, L.F.; Mao, Y.S. Parameter identification of unmanned marine vehicle manoeuvring model based on extended kalman filter and support vector machine. *Int. J. Adv. Robot. Syst.* **2019**, *16*. [[CrossRef](#)]
- Moreira, L.; Soares, C.G. Dynamic model of manoeuvrability using recursive neural networks. *Ocean Eng.* **2003**, *30*, 1669–1697. [[CrossRef](#)]
- Zhang, G.Q.; Zhang, X.K.; Pang, H.S. Multi-innovation auto-constructed least squares identification for 4 dof ship manoeuvring modelling with full-scale trial data. *ISA Trans.* **2015**, *58*, 186–195. [[CrossRef](#)]
- Liang, C.L.; Zhang, X.K.; Watanabe, Y.; Zhao, B.G. Novel I+ and fo I+ algorithms based on enc data for automatic route planning of ships. *Ocean Eng.* **2021**, *235*, 186–195. [[CrossRef](#)]
- Zhao, B.G.; Zhang, X.K. An improved nonlinear innovation-based parameter identification algorithm for ship models. *J. Navig.* **2021**, *74*, 549–557. [[CrossRef](#)]
- Zhao, B.G.; Zhang, X.K.; Liang, C.L. A novel path-following control algorithm for surface vessels based on global course constraint and nonlinear feedback technology. *Appl. Ocean Res.* **2021**, *111*, 102635. [[CrossRef](#)]
- Liang, C.L.; Zhang, X.K.; Han, X. Route planning and track keeping control for ships based on the leader -vertex ant colony and nonlinear feedback algorithms. *Appl. Ocean Res.* **2020**, *101*, 102239. [[CrossRef](#)]
- Yasukawa, H.; Sakuno, R. Application of the mmg method for the prediction of steady sailing condition and course stability of a ship under external disturbances. *J. Mar. Sci. Tech. -Jpn.* **2020**, *25*, 196–220. [[CrossRef](#)]
- Yasukawa, H.; Hirata, N.; Matsumoto, A.; Kuroiwa, R.; Mizokami, S. Evaluations of wave-induced steady forces and turning motion of a full hull ship in waves. *J. Mar. Sci. Tech. -Jpn.* **2019**, *24*, 1–15. [[CrossRef](#)]